Seismic arrays at Deception Island 1998-99 survey - 1st phase.

Gilberto Saccorotti, Javier Almendros, Enrique Carmona, Jesus Ibanez and Edoardo Del Pezzo

Partecipating Institutions:

1. Instituto Andaluz de Geofisica - Granada, Spain.
2. Instituto Geografico Nacional - Spain
3. Dipartimento di Fisica dell'Università degli Studi di Salerno – Salerno, Italy
4. Osservatorio Vesuviano – Napoli, Italy

ABSTRACT

The contents of this report describe the operation of two short-period seismic arrays deployed at Deception volcano, Southern Shetland Island, Antarctica, in the framework of the Spanish project '*Sismicidad volcanica, local y regional del area de las Shetland del Sur y Estrecho de Bransfield, ANT98-111*'. The two arrays were installed during the 1998-1999 austral summer, and were aimed to a quantitative assessment of the complex wavefields associated to the volcanic and hydrothermal activity of the volcano. The twin-array deployment was complemented by two continuos recording, mobile digital stations. During the first phase of operation (from December 1998 to early January 1999), the deployments recorded several regional earthquakes related to the complex dynamics of the Bransfield Strait and adjoning areas. Signals of local origin were classified according to their duration, amplitude, and frequency content. We identified signals related to the activity of a shallow hydrothermal system, and low-energy ice-quakes associated to the ice-melting processes. The kinematic properties of some selected records of background noise, long-period events, regional and local earthquakes are investigated using the zero lag, average cross-correlation method. Under the assumption that the wavefield of the background seismic noise is dominated by scattered surface waves, we apply the statistical method of Aki (1957) to investigate the dispersion properties of Rayleigh waves in the 1-8 Hz frequency band. The results clearly show that the two sites selected for the array deployments are characterized by a marked difference in the dispersive properties of the medium. At the beginning of January, 1999, a significant increase in the rate of occurence of local earthquakes began, rapidly leading to the build-up of one of the most energetic seismic crisis ever recorded on the island.

1. INTRODUCTION

Deception Island (62º59'S, 60º41'W), located northwest of the Antarctic Peninsula, is the main active volcano of the marginal trench of the Bransfield strait. The first seismic observations at Deception Island date back to 1986; moreover, since 1994 the island has been monitored during the austral summers using a dense, small aperture array located in the close neighborhood of the Spanish geophysical observatory '*Gabriel De Castilla*'.

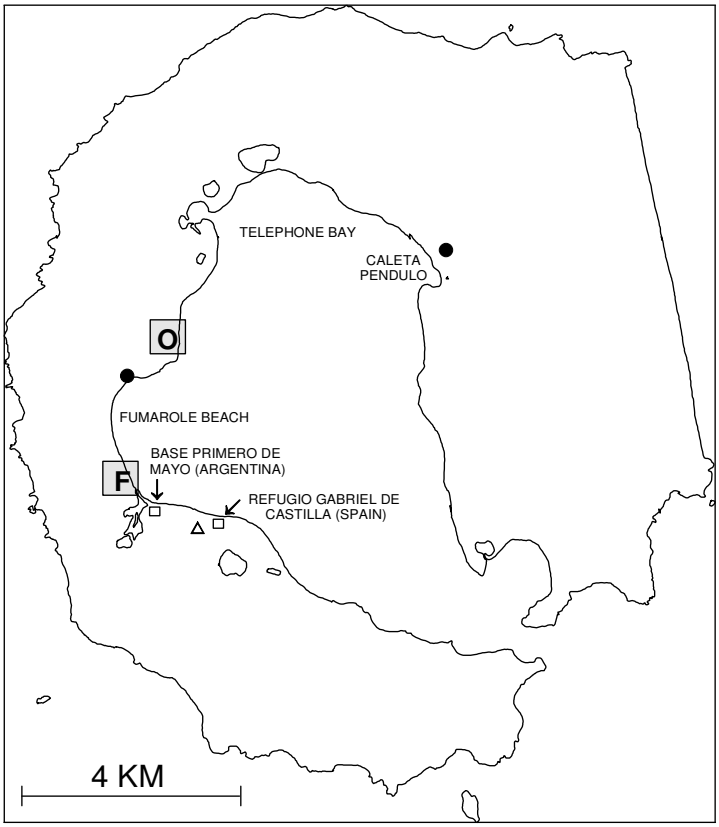

Fig. 1 - Map of Deception Island, with location of the Spanish base Gabriel de Castilla and the Argentinian base Primero de Mayo. The two shaded areas mark the location of the Obsidiana (O) and Fumarole (F) arrays. Black dots mark the position successively occupied by the vertical-component mobile seismic station. The triangle marks the location of the fixed, three component station BASE. The 1969-1970 volcanic activity occurred along a fracture and fissure system extending from Telephone bay to Caleta Pendulo .

These experiments contributed important progresses in the knowledge of the wavefield composition and source location of the local and regional seismicity, also offering new glimpses into the interpretation of the corresponding source processes. These past studies also demonstrated the usefulness of dense, small-aperture arrays in the discrimination and analyses of seismic signals related to the volcanic and hydrothermal acitivity at Deception island, and suggested the need of extending the observations to other sector of the volcano, with special reference to the N-NE inner shore of the caldera where the most recent eruptive activity occured.

This goal has been attained with the 1998-99 seismic survey, during which two seismic arrays have been deployed at a distance of about 4 and 7 km from the western edge of the eruptive fissure which produced the 1969-1970 phreato-magmatic activity (Fig. 1). Two continuous-recording stations complemented the deployment. The contents of this report describe the operation of the twin-array and single-stations setups, and the preliminary results from the analyses of some selected records of background noise and transient signals associated to different sources.

2. SITES SELECTION ; ARRAYS SETUP AND CONFIGURATION

The selection of the sites for the installation of the twin-array setup was mostly costrained by the topography and the accessibility for array maintainance and data retrieval.
Sensor positioning at both the array was determined using a digital total station. We first measured station coordinates respect to the magnetic north, and then rotated this preliminary coordinates by 14 degrees westward, assuming that that was the average value for the magnetic declination (Table I and II).

The first array was installed in the Obsidianas beach, about 3 km south-south west of the craters formed during the 1970 activity (see Fig. 1). This array consisted of 14 stations deployed along two concentric circles of radius 160 and 80 m, respectively (Fig. 2). Stations at the external and internal

semicircle were spaced by angular intervals of about 26 and 45 degrees, respectively, with respect to the hub of the array. We couldn't achieve either a regular angular- and distance-spacing between stations due to the high number of thaw-water gulleys and streams crossing the bay.
Station at the hub of the array was equipped with a 3-component, L-15 Mark sensor. All the other stations were equipped with vertical component, L-15 Mark sensors, all having a natural frequency of 4.5 Hz. Electronic extensions allowed to all the sensors to achieve a flat response curve in the 1-50 Hz frequency interval.

Table I - Station coordinates of the Obsidiana array referred to the hub of the array.

Station name	x (m)	y (m)	z (m)
3cm	0	0	0
1n	-12.76401	-172.3898	-0.39
2n	-99.19614	-124.956	1.805
3n	-173.5178	-83.5954	3.6
4n	-163.0675	-9.811862	4.83
5n	-156.08	53.36121	4.514
7m	-141.5048	83.98789	3.95
6m	-69.12511	151.4588	2.42
5m	25.67822	163.7159	-0.68
4m	12.67704	84.82275	-0.35
8m	-56.13249	63.68952	1.766
6n	-81.46378	-3.571213	2.344
7n	-58.5127	-53.28014	1.433
8n	-13.82391	-80.34941	0.147

Table II - Station coordinates of the Fumarolas array referred to the hub of the array.

Station name	x (m)	y (m)	z (m)
zf1	0	0	0
zg3	-41.83791	-43.67585	4.714
zf2	-55.96347	23.09789	-0.979
8g	-17.00284	57.70134	-4.438
8f	-34.31166	114.8493	-6.741
7f	-105.9478	60.48783	2.345
7g	-119.0063	-23.64515	4.869
5g	-63.88645	-102.933	10.21
4g	13.87942	-59.54755	0.632
6g	41.9468	-113.8847	0.957
6ga	31.41171	-136.0082	4.577

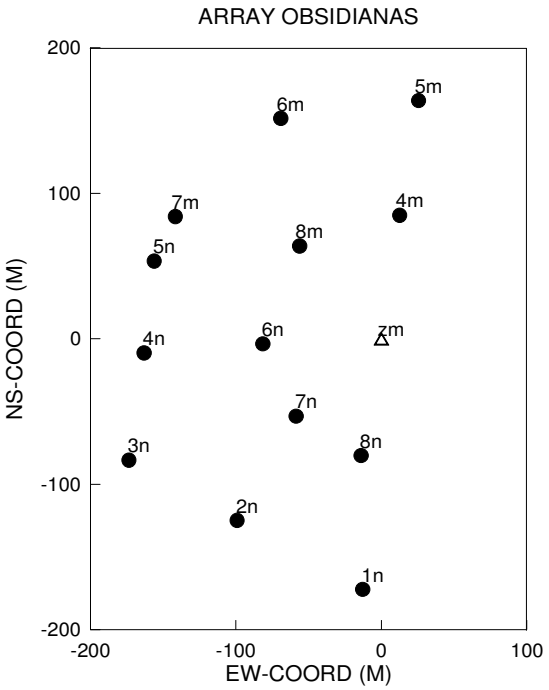

Fig. 2 - Configuration of the Obsidiana array. Solid dots mark vertical-component sensors, and the triangle at the hub of the array marks the three-component seismometer.

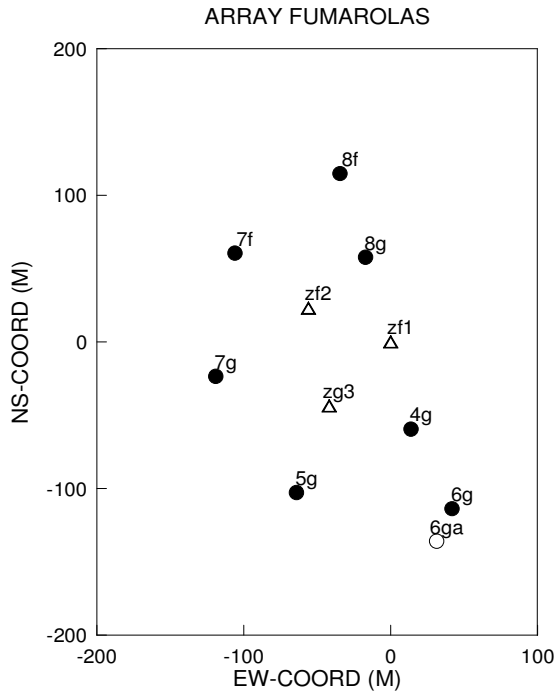

Fig. 3 - Configuration of the Fumarolas array. Solid dots mark vertical-component sensors, and triangles indicate the three-component seismometers.

The second array was deployed atop of an alluvial fan in close proximity of the Fumarole Bay fumarole system, approximately 500 m N-NE of the Argentinian base (see Fig. 1). This array had an aperture of approximately 240 m with station located along two semicircle, one of radius 120 m and the other of radius 60 m (Fig. 3). The angular spacing between stations of the outer semicircle was of 45 deg, and of 60 deg for the inner semicircle. This array was equipped with three Mark L4 three-component sensors having a natural frequency of 1 Hz and a sensitivity of 1 V/m/s, and with 7 Mark L15 vertical sensors having the same characteristics as the ones previously described for the Obsidiana array. The Obsidiana array started its operation on December 9, 1998, and the Fumarolas array on December16, 1998.

Approximately at 23 UT on Dec. 20, 1998, we moved one station from site 6ga to site 6g. Station 5g of the Fumarola array had a reversed polarity from the beginning of the recordings up to 22h (UT) on January 1, 1999.

Recording at each array was performed via two eight-channel, PC-based digital recorders with a dynamic range of 16 bits, storing data at 200 samples/second/channel. The instruments were programmed to record in trigger mode, according to the STA-LTA algorythm. In addition, 150-s-long sections of background noise were periodically recorded at both the arrays.

3. DATA DESCRIPTION AND ANALYSES

The data-set recorded by the twin-array deployment includes a variety of seismic signals which have been preliminary classified according to their shape, magnitude, and frequency content. In the following section we shortly describe the different type of signals, and use array-averaged power spectra to explore their mutual relationships and short-term evolution. The kinematic parameters of the wavefields of some selected records from the different classes of signals are then investigated using the Maximum Average zero-lag Cross Correlation (MACC) method. Finally, we apply the

correlation method of Aki (1957, 1965) to background noise records from both the arrays to measure the phas e velocities and dispersion properties of Rayleigh waves in the 0.5-8 Hz frequency band.

3.1. Tectonic Earthquakes

We classified as tectonic earthquakes signals characterized by a frequency content betweeen 5 and 20 Hz, a duration in the 5-50 s range, and a clear P- and S-wave onsets. Most of the tectonic earthquakes we recorded depict an S-P delay time in the 5-8 s range, indicative of epicentral distances in the order of a few tenths of kilometers. Starting on Dec. 29, 1998, the rate of occurence of eathquakes increased, and we began to observe also very local events, characterized by an S-P delay time shorter than 1 s.

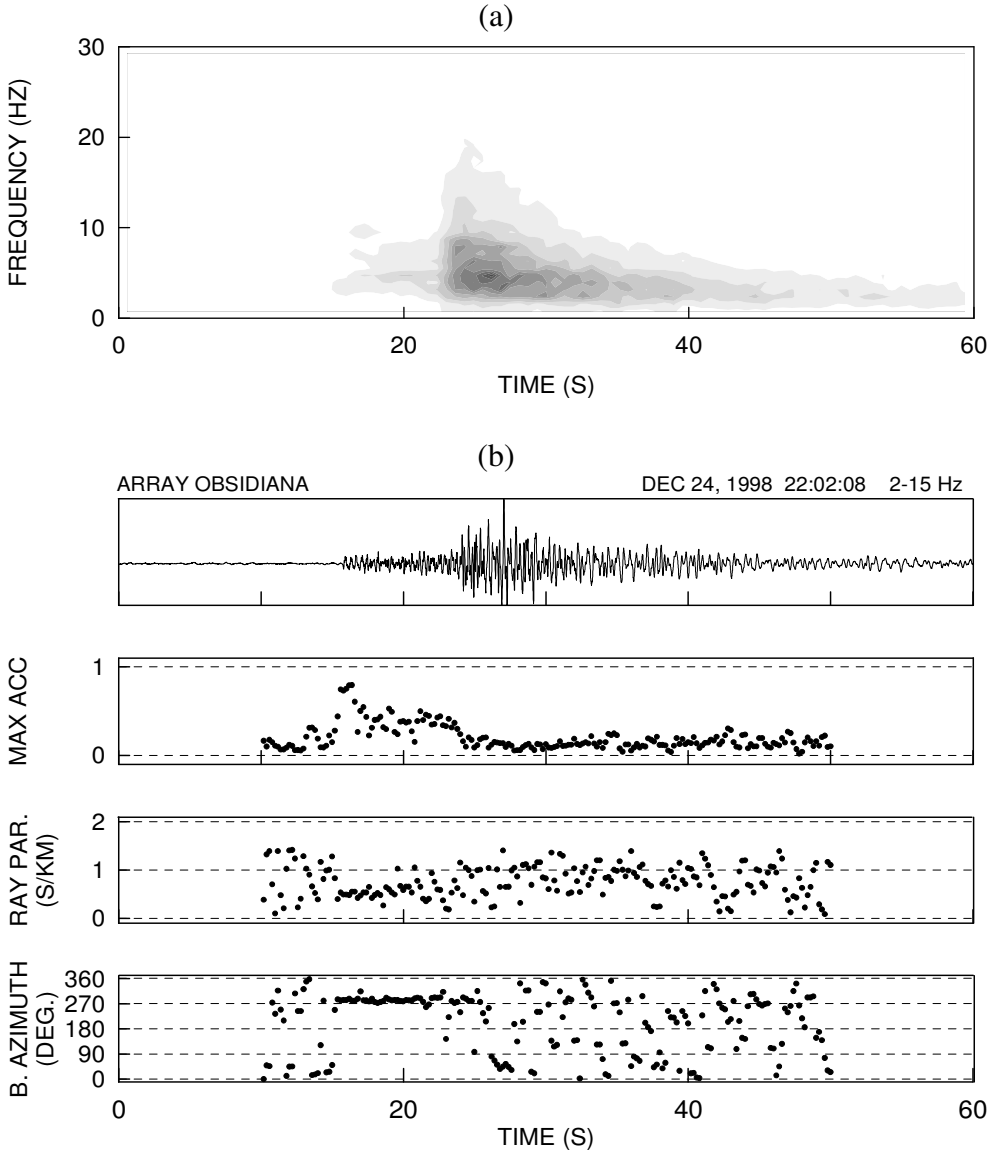

Fig 4 - a) array-averaged spectrogram of a regional earthquake recorded at the Obsidianas array on December 24, 1998. b) From top to bottom : unfiltered trace of the vertical component of ground velocity at station MZ, located at the hub of the array ; Time-dependance of the average zero-lag cross-correlation coefficient obtained from analyses of the traces of all the vertical stations of the array ; horizontal slowness (ray parameter) corresponding to the maximum of the MACC; back azimuths of the maximum of the MACC. Date and time at the start of the records, and the frequency band over which the MACC analysis has been conducted are reported at the upper right corner of the figure.

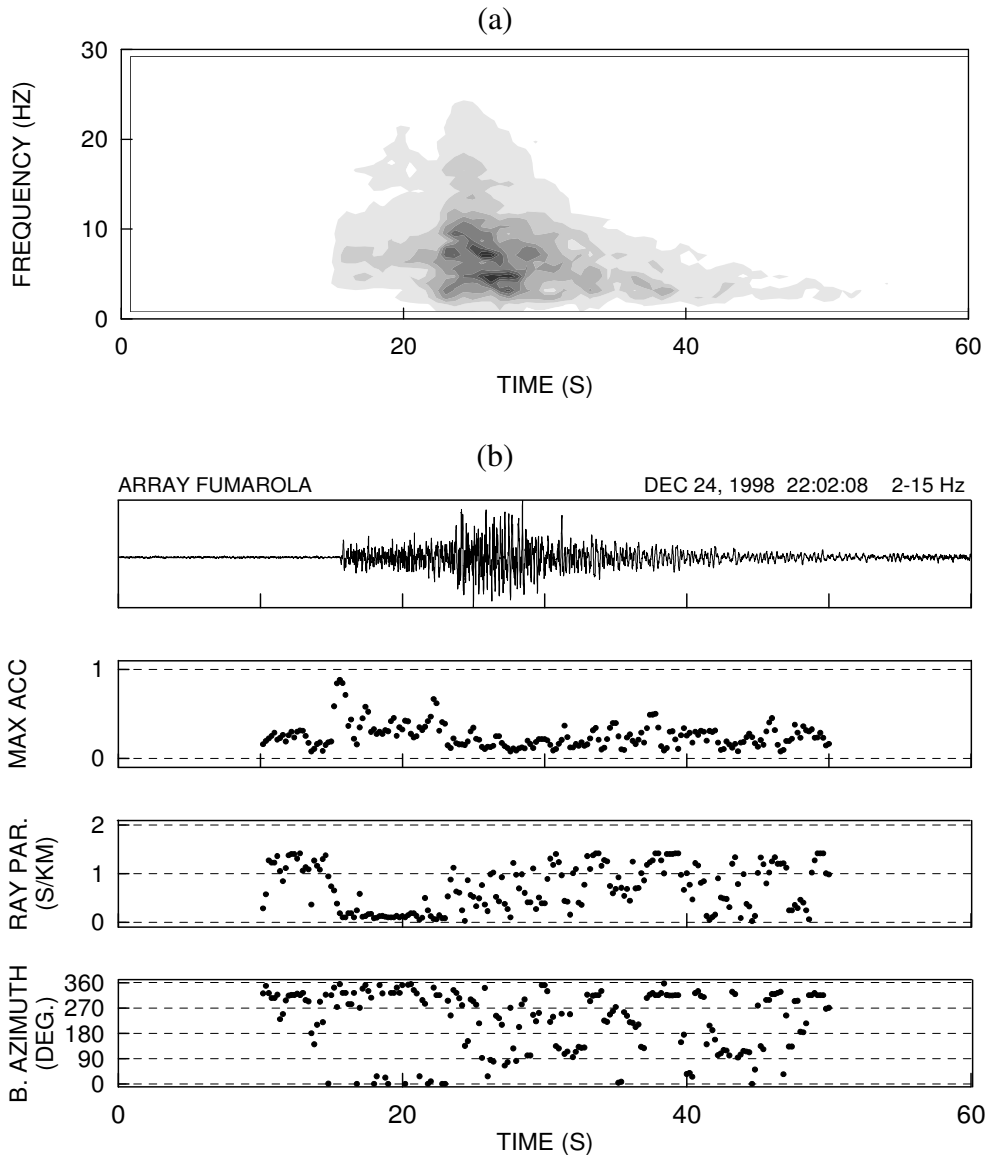

Fig 5 - The same as in figure 4, but for the Fumarolas array.

3.2. Long-period events

The long-period events are a typical signature of the seismo-volcanic activity, and have been recorded in the island during the past surveys. Now we find them in both the Fumarolas and Obsidianas arrays. The main characteristics are:

- Almost monochromatic spectral content in the range 1-4 Hz.
- Spindle-shaped envelope
- Short duration (in the order of 5-15 s)

(a)

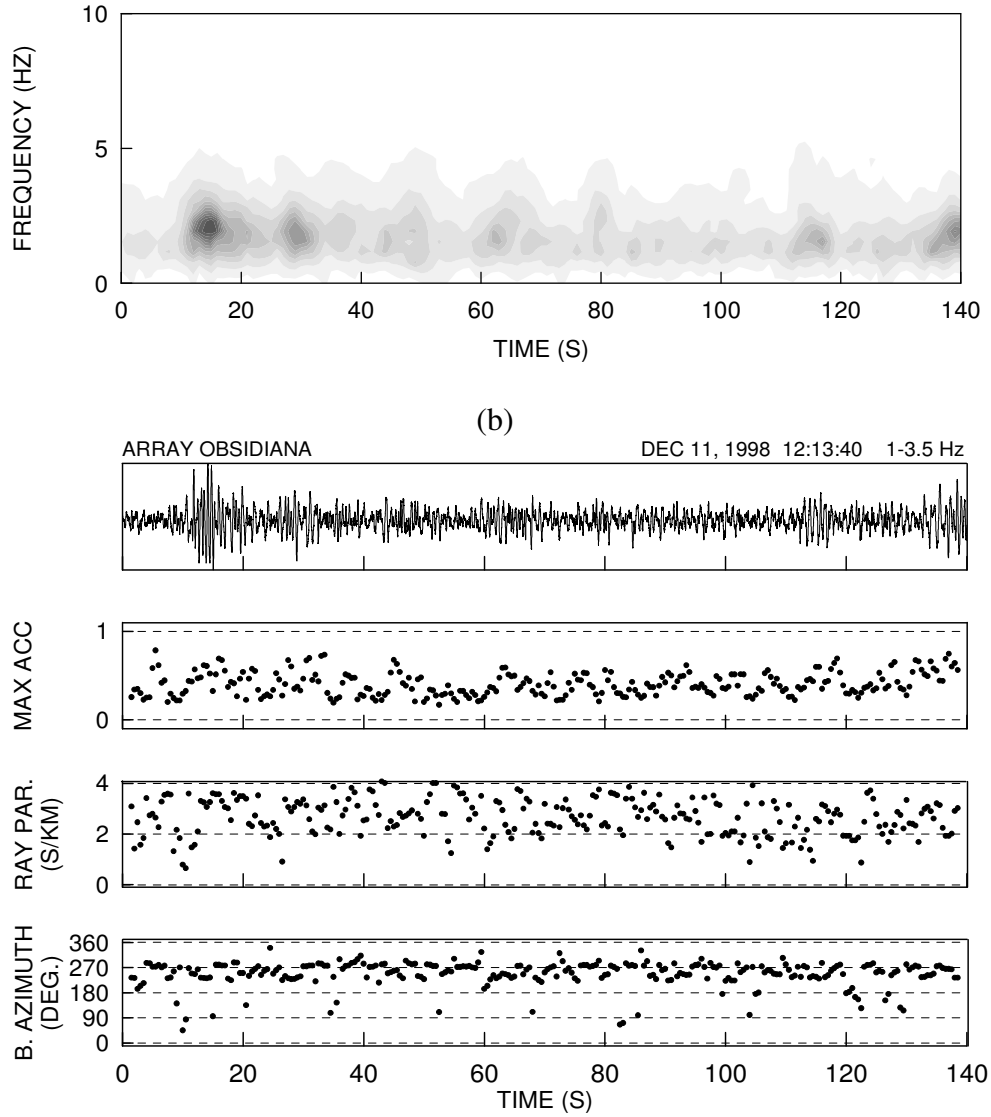

Fig 6 -The same as in figures, 4 and 5 but for two long-period bursts recorded at the Obsidiana array.

3.3. Events of unknown origin

There are many events, mainly recorded at Obsidianas array, characterized by:

- High-frequency content (10-30 Hz).
- Short duration (tipically 1 s).
- Fast attenuation, even along very short distances.
- Slow propagation across the array.

An hypothesis about the origin of these events is that they are caused by rocks and ice-blocks falling related to the snow- and ice-melting processings

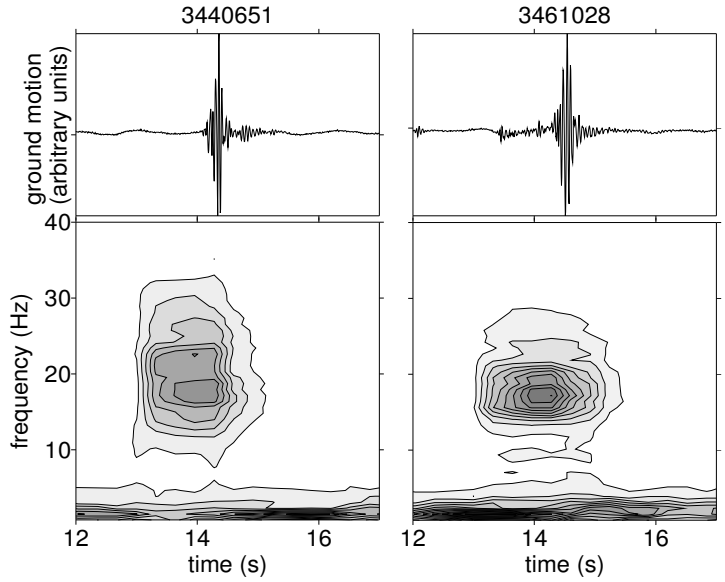

Fig. 7 - Array - averaged spectrograms for two High-frequency events recorded at the Obsidiana Array. Array-averaged spectra have been calculated over 1.28-s-long windows shifting through the signal with increments of 0.32 seconds.

3.3 Correlation analysis and noise properties

Background noise records from both the array were analyzed using the correlation method of Aki (1957, 1965). Assuming that microtremors represent the sum of horizontally propagating waves that have the same phase velocity for a given frequency and that waves propagating in different directions are statistically independent, the phase velocity can be related to an azimuthal average of the spatial correlation. Aki (1957, 1965) shows that, given a semicircular array of stations with a sensor at the centre of the semicircle, a spatial correlation function $\phi(r, \varphi)$ can be defined as :

$$\phi(r, \varphi) = < u(x,y,t)\, u(x + r\cos\varphi, y + r\sin\varphi, t) > \quad (1)$$

where $u(x,y,t)$ is the ground velocity observed at point (x,y) and time t ; r is the station separation ; φ is the station azimuth, and <> denotes the ensamble (time) average. The azimuthal average of this function is given by :

$$\phi(r) = \frac{1}{\pi}\int_0^{\pi} \phi(r,\varphi)\, d\varphi \quad (2)$$

For the vertical component, the power spectrum, $\phi(\omega)$, can be related to $\phi(r)$ via the zeroth order Hankel transform :

$$\phi(r) = \frac{1}{\pi}\int_0^{\infty} \phi(\omega) Jo\left(\frac{\omega}{c(\omega)} r\right) d\omega \quad (3)$$

where ω is the angular frequency and $c(\omega)$ is the frequency-dependent phase velocity. If noise recordings from the array are band-pass filtered over a narrow frequency band centered on ω_o and $\phi(r)$ is computed for the filtered series, then the normalized spatial correlation function will be of the form :

$$\phi(r) = Jo\left(\frac{2\pi\omega_o r}{c(\omega)}\right) \quad (4)$$

Thus, phase velocities estimates can be made from measurements of correlation functions for vertical motion from a semicircular array. Equations (1) to (4) are valid for the vertical component of motion, which will consist of P-SV motion. Assuming that ambient noise is comprised mainly of surface waves, the results from application of these equations can be interpreted as an estimate of Rayleigh-waves phase velocities.

In our analyses, we first selected 16000-sample-long time series (1' 20") of background noise recorded at all the stations of the array (Fig. 8). The time series for each station of the array were then fourier-transformed, and the complex spectrum windowed using a 0.5 Hz-width boxcar function. We then calculated the inverse fourier transform and, once back in the time domain, calculated the zero-lag correlation coefficient of the signal from the station located at the hub of the array and the stations located at the two semicircles. The frequency-dependent correlation coefficient thus obtained were finally averaged among stations located at the same distance from the hub of the array. This procedure was then repeated by shifting the frequency window with 0.125 Hz steps, in the 0.5-8 Hz interval. To improve the significance of the estimates, we then repeated the calculus over 6 noise windows, recorded between the Julian day 344-351 for the Obsidiana array and day 349-361 for the Fumarolas array (Table II).

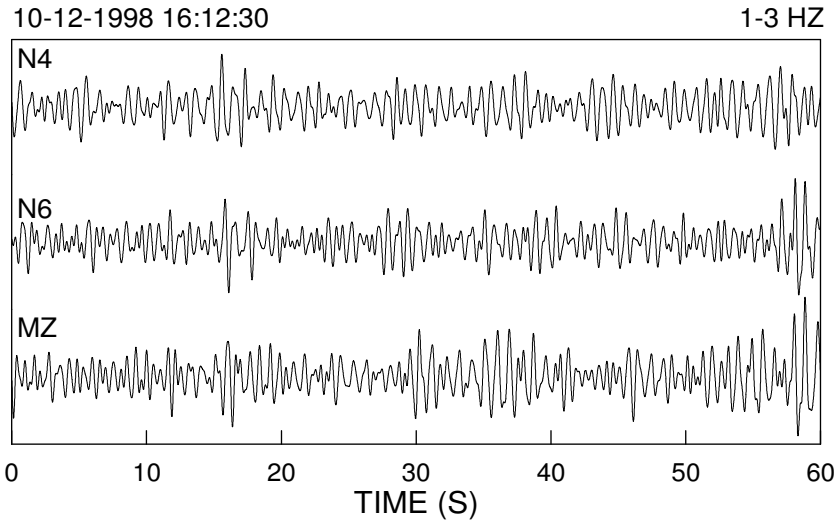

Fig. 8 - 1-minute long record of the vertical component of ground motion for background noise recorded at stations N4, N6 and MZ of the Obsidiana Array (see Fig. 2). Traces have been band-pass filtered in the 1-3 Hz frequency band.

Table III- Array *Obsidianas* : Selected recordings for correlation analyses

File Name	*Date of record*	*Start time of record, module M (UT)*	*Start time of record, module N (UT)*	*Start time of analysis (UT)*
3441612	10-12-98	16 :12 :10	16 :12 :10	16 :12 :10
3452326	11-12-98	23 :26 :14	23 :26 :42	23 :27 :22
3460410	12-12-98	04 :10 :15	04 :10 :14	04 :10 :15
3470445	13-12-98	04 :45 :38	04 :45 :37	04 :45 :58
3492113	15-12-98	21 :13 :54	21 ;13 :54	21 :14 :29
3502229	16-12-98	22 :29 :13	22 :29 :12	22 :29 :48

Table IV - Array *Fumarolas* : Selected recordings for correlation analyses

File Name	*Date of record*	*Start time of record, module M (UT)*	*Start time of record, module N (UT)*	*Start time of analysis (UT)*
3491719	15-12-98	17 :19 :16	17 :19 :16	17 :19 :16
3542312	20-12-98	23 :12 :28	23 :12 :28	23 :12 :28
3550445	21-12-98	04 :45 :41	04 :45 :42	04 :45 :42
3572038	23-12-98	20 :38 :26	20 :38 :26	20 :38 :26
3582227	24-12-98	22 :27 :11	22 :27 :11	22 :27 :11
3612300	27-12-98	23 :00 :44	23 :00 :44	23 :01 :28

3.3.1 Results

The frequency dependence of the correlation coefficient averaged over the stations of the two semicircles of the Obsidiana Array are shown in Figure 9 for the twelve different data windows analyzed. In analyzing data from the external semicircle (r = 160 m), we omitted station 3N, whose distance from the hub of the array was sensitively different from the average distances of the other sites.

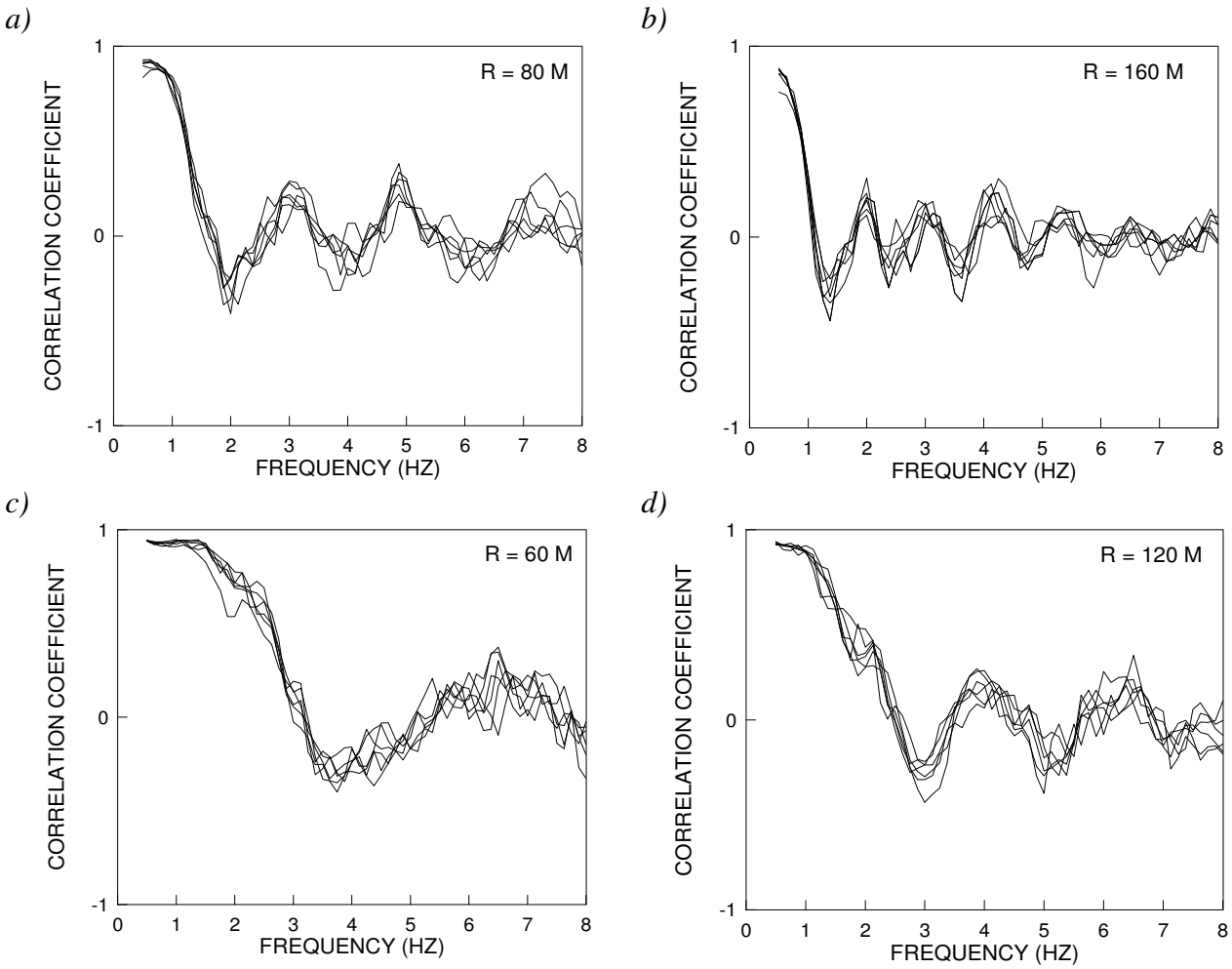

Fig. 9 - frequency dependence of the azimuthally-averaged correlation coefficient for the inner (a) and outer (b) semicircles of the Obsidiana Array. In (c) and (d) the corresponding results for the Fumarolas array are shown.

From the average of the curves shown in Figure 9, we derived the frequencies correspondent to the maxima, minima and zero crossings of the azimuthally averaged correlation functions. These values are then equaled to the corresponding arguments of the zeroth order Bessel function of eq. (4), to

derive the values of the frequency-dependent phase velocity *c(f)* (Fig. 10). The reading of zero crossing, maxima and minima was extended up to 8 Hz for the correlation functions obtained from the smaller semicircle, and up to 5.5 Hz for those obtained from the larger semicircle.

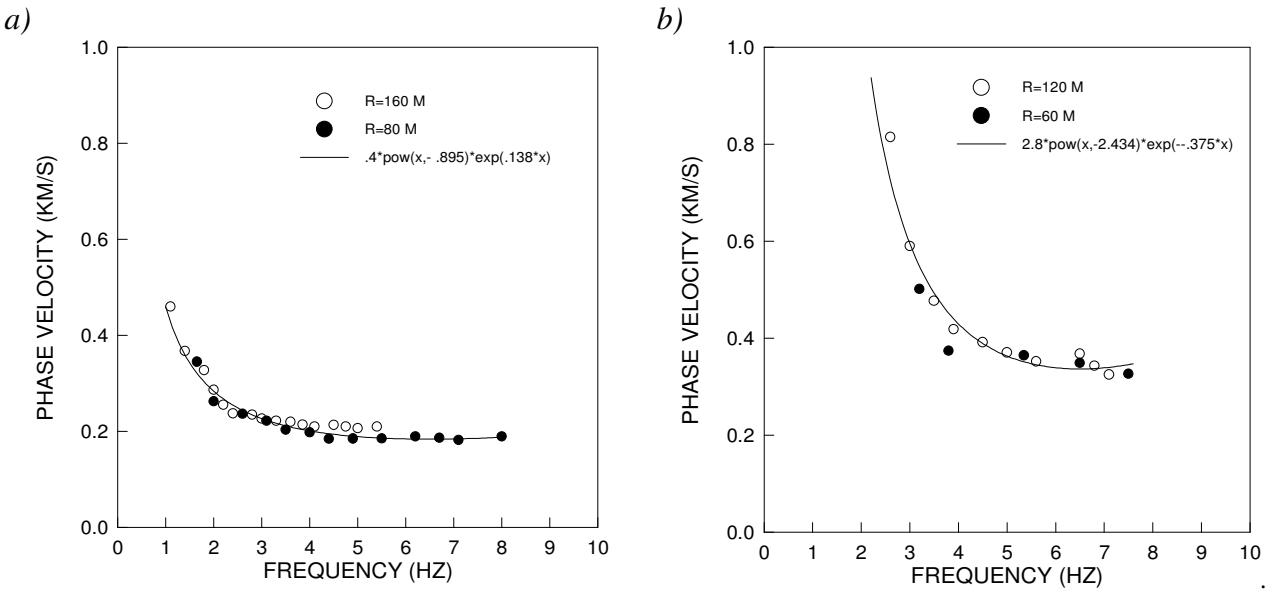

Fig. 10. (a) Phase velocities as a function of frequency for the P-SV component of motion derived at the Obsidiana Array. Solid dots are solutions from application of eq (4) to azimuthally averaged cross-correlation coefficients relative to the inner semicircle.Empty dots mark the solutions obtained from the outer semicircle. (b) The same as in (a), but for the Fumarolas array.

The dependences of phase velocities on frequency shown in Figure 10 are then least-squares fitted using a relationship of the form

$$c(f) = C\ f^{-a}\ e^{\,bf}, \tag{5}$$

where f is the frequency, in Hertz, and C, a and b are constants. For the Obsidiana site, C=0.4, a=0.866 and b=0.133 ; For the Fumarolas site, C=2.8, a=2.434 and b=-0.375.

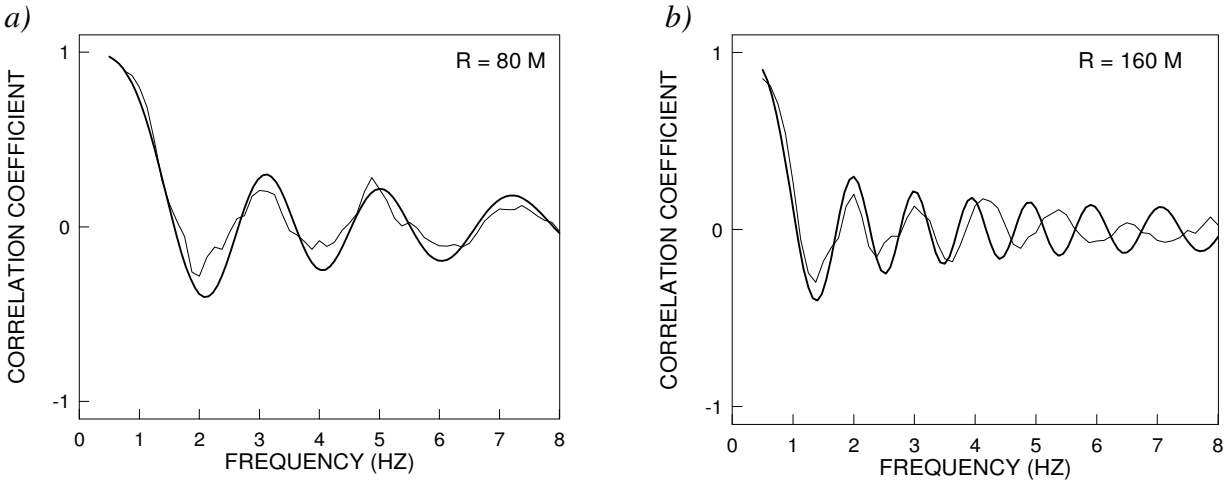

c) d)

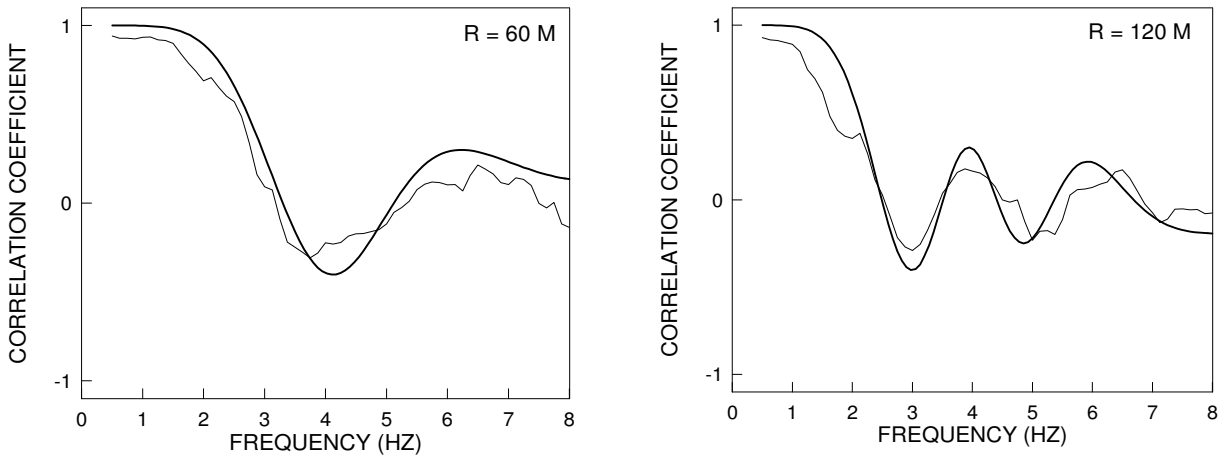

Fig. 11. Azimuthally averaged correlation functions for the 80-m- (a) and the 160-m-long array radii (b). The thin line is the experimental function obtained from average over the six different data windows listed in Table III. The thick line represent the 0^{th} order Bessel function obtained by substitution of the dispersion relationship expressed through equation (5) to the phase velocity terms at the right-hand side of equation (4). (c) and (d) : the same as for (a) and (b), but referred to the inner and outer semicircle of the Fumarolas array. The experimental lines are the average of the azimuthally averaged correlation functions obtained over the six data windows listed in Table IV.

Finally, the least-squares functions expressed through equation (5) were substituted into eq. (4) to calculate the frequency-dependent argument of the Bessel function ; this allows for an *a posteriori* verification of the goodness of the fit between the model (the 0^{th} order bessel function) and the data (the frequency-dependent, azimuthally averaged correlation coefficients for a given distance - Fig. 11).

The kinematic parameters of the seismic noise have also been investigated using the MACC method. At both the Obsidianas and Fumarolas array the background noise is confined in a narrow frequency band focused at frequency 1 Hz; for this reason, we applied the MACC analyses to noise records filtered in the 0.5-2 Hz frequency band. The results from these analyses are shown in Figures 12 and 13.

(a)

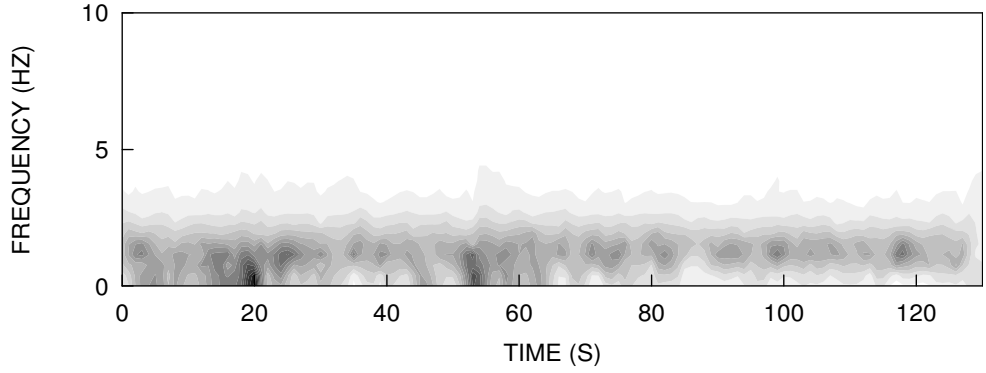

(b)

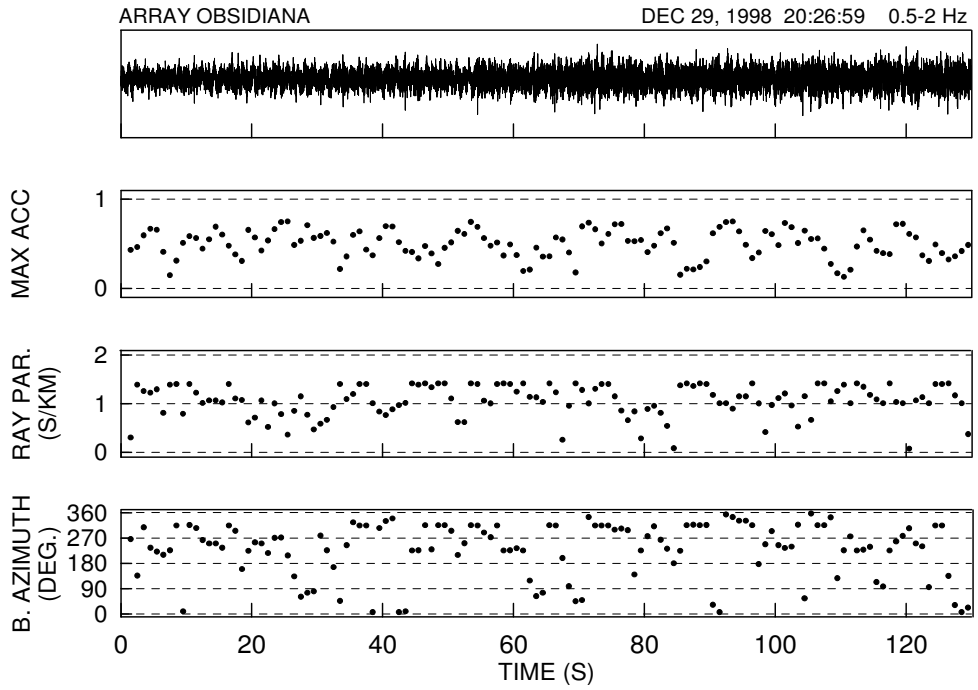

Fig 12 -The same as in figures, 4,5 and 6 but for a background noise section recorded at the Obsidiana array.

4. CONTINUOUS-RECORDING STATIONS

Two continuous-recording stations were deployed during the survey. The first station (BASE) was installed in the close neighborhood of the base. This station was equipped with a three-component Mark L4-C sensor with a natural frequency of 1 Hz and a sensitivity of 1 V/m/s. Continuous recording was performed via a PC-based system with a dynamic range of 24 bits and a sampling rate of 50 samples/second/channel.

With the aim of detecting the level of the very-local seismicity at different sites of the island, the second continuous recording station was installed at different sites. This station was equipped with a vertical-component, Mark L4 sensor with a natural frequency of 1 Hz and a \sensitivity of 1 V/m/s. Continuous recording at this station was performed via a PC-based system with a dynamic range of 24 bits and a sampling rate of 50 samples/second/channel. In Table V the coordinate and operating period of the mobile station at each different site are listed.

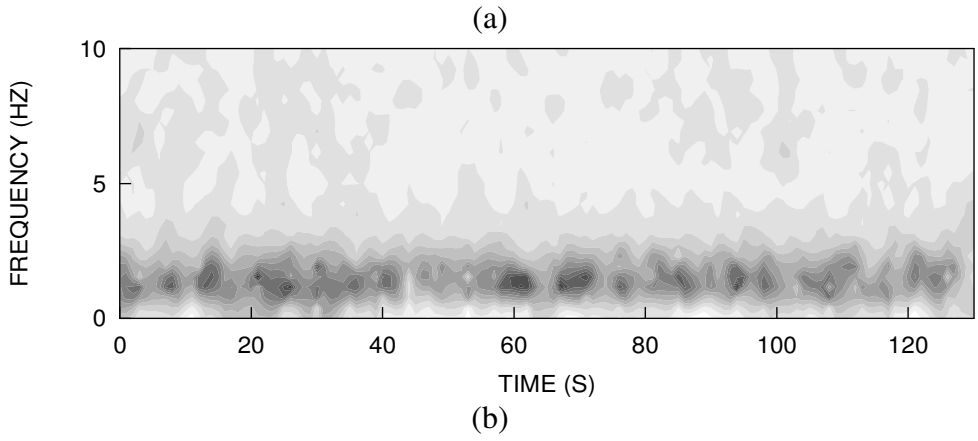

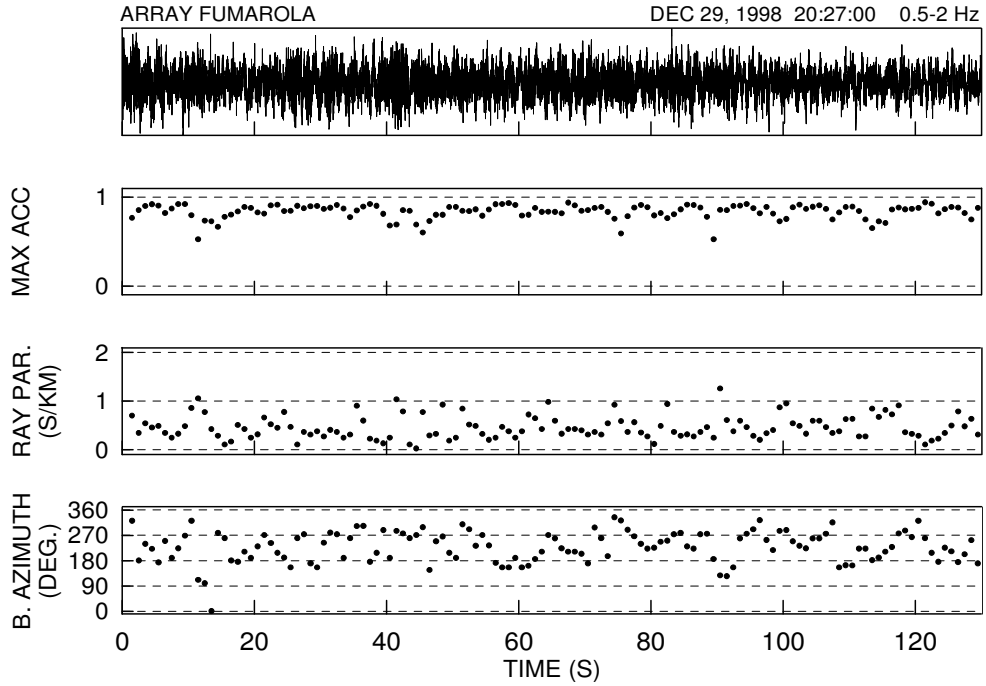

Fig 13 -The same record of background noise as in Fig. 12, but for the Fumarolas array.

Table IV - Mobile station: coordinates and periods of operation

Site name	*Latitude*	*Longitude*	*Date at the beginning of record*	*Date at the end of record*
Base (BASE)			Dec. 4 1998	-
Fumarola (FUMA)	62 57' 16" S	60 42' 31" W	Dec. 15 1998	Dec. 23 1998
Pendulo (PEND)	62 56' 10" S	60 35' 34" W	Dec. 29 1998	-

4.1 Spectrograms

The first step in analyzing data from the continuous recording stations was to extract 1-hour-long data sections from the continuous data stream. On these sections, we derived hourly-averaged power spectral densities by *a)* calculating power spectra over a 16.38-second-long window (8192 samples) shifting through the signals with increments of 8.19 s (4096 samples), then by *b)* averaging the different spectra thus obtained, and finally *c)* averaging the results with a 11-samples (approximately 0.06 Hz) boxcar window. Examples of this procedure for the BASE, FUMA and PEND stations are shown in Figures 14. In these figures, blanked areas are indicative of extremely low values of thespectral power, which cannot be represented due to the low colour range of the displaying program.

a)

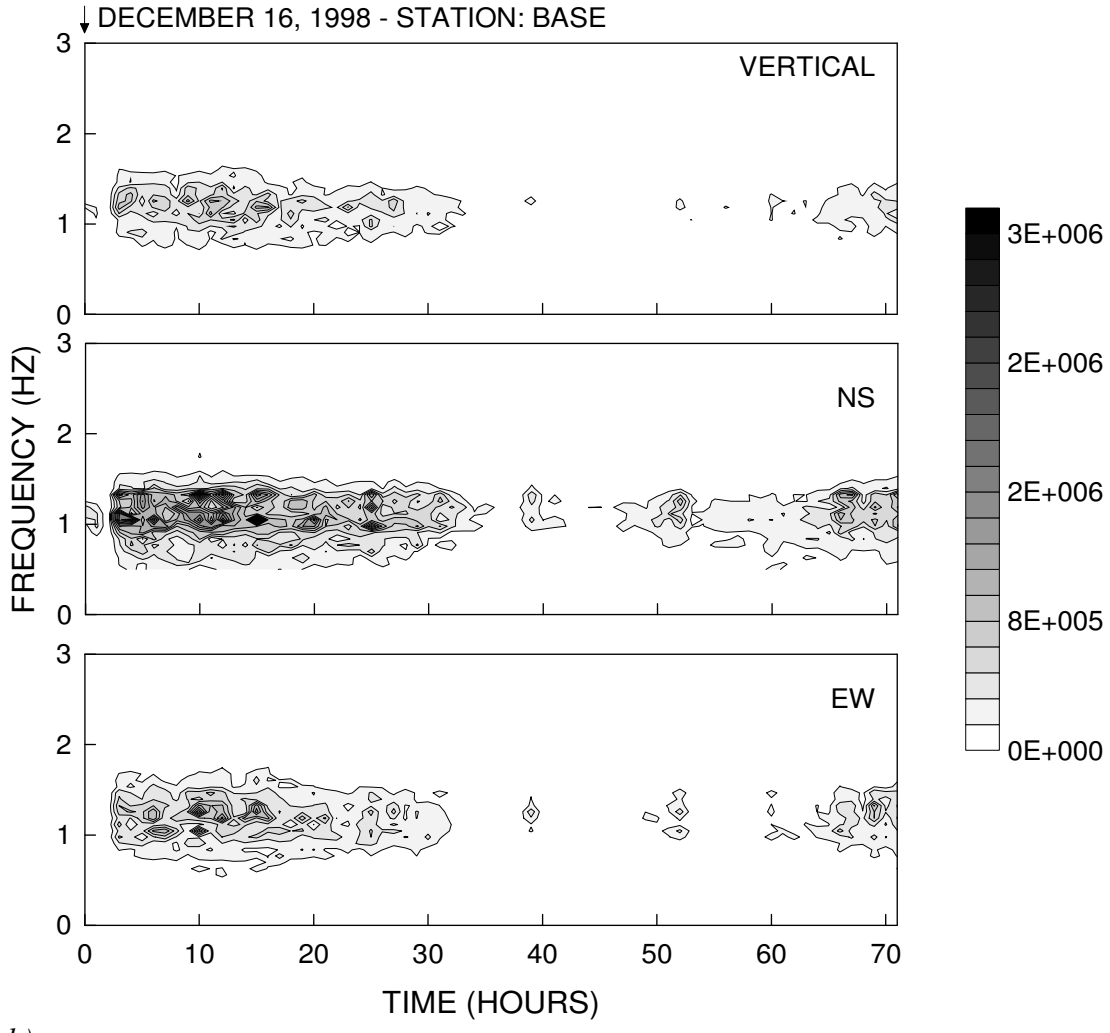

b)

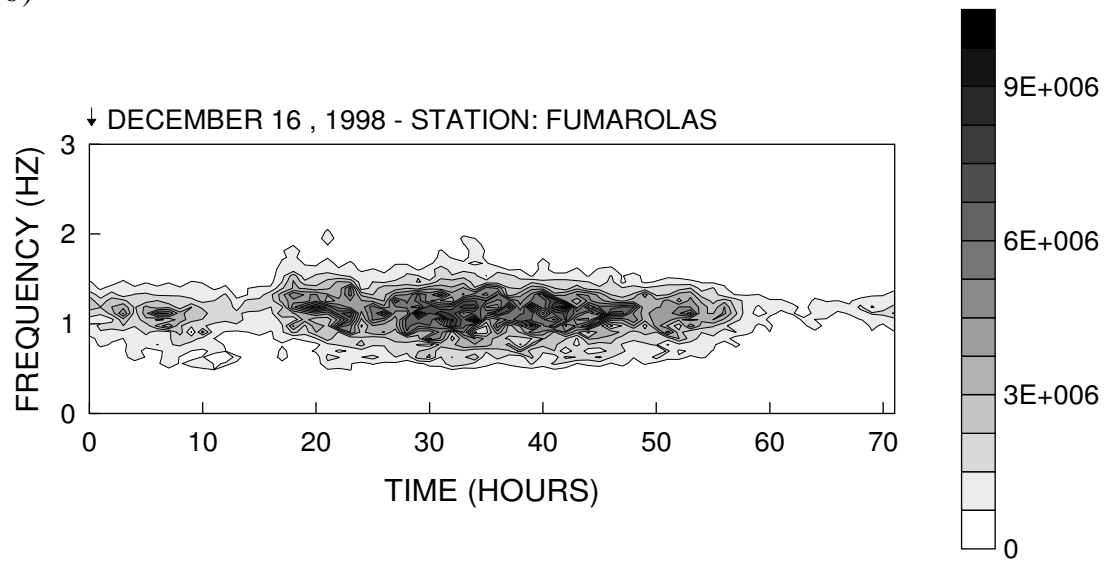

Fig. 14 - Spectral power as a function of time and frequency (spectrograms) derived from (a) the three components of ground velocity at the continuous recording station BASE, located in close proximity of the Spanish Base 'Gabriel de Castilla', and (b) at the northern edge of the Fumarolas beach (see Fig. 1). The two spectrograms refers to the same time interval, as depicted by the date at the left top of each plot..

REFERENCES

Aki K., 1957. Space and Time Spectra of Stationary Stochastic Waves, with special reference to microtremors. *Bull. Earthq. Res. Inst. Tokio Univ*., 25, 415-457.

AKNOWLEDGEMENTS

The scientific expedition at Deception Island has been supported by the project ANT98-111 under the Spanish Antarctic Research Program. This work could have not been possible without the logistic and technical assistance of the military staff of the Gabriel de Castilla base. Jaime Potti, Ana de Leon, Juanto Fargallo, Mariano Rodriguez-Arias and Fernando Calexico are greatfully aknowledged for their friendship and moral support.